Atomic Data and Nuclear Data Tables 105–106 (2015) 1–8

Contents lists available at ScienceDirect

Atomic Data and Nuclear Data Tables

journal homepage: www.elsevier.com/locate/adt

Vanadium fine-structure K-shell electron impact ionization cross sections for fast-electron diagnostic in laser–solid experiments

P. Palmeri [a,*], P. Quinet [a,b], D. Batani [c]

[a] Astrophysique et Spectroscopie, Université de Mons - UMONS, B-7000 Mons, Belgium
[b] IPNAS, Université de Liège, B-4000 Liège, Belgium
[c] CELIA, Université de Bordeaux, F-33400 Talence, France

ARTICLE INFO

Article history:
Received 23 February 2015
Accepted 26 April 2015
Available online 19 May 2015

Keywords:
Atomic processes
Electron impact ionization
Inner-shells
Hot plasmas
High densities
Relativistic effects

ABSTRACT

The K-shell electron impact ionization (EII) cross section, along with the K-shell fluorescence yield, is one of the key atomic parameters for fast-electron diagnostic in laser–solid experiments through the K-shell emission cross section. In addition, in a campaign dedicated to the modeling of the K lines of astrophysical interest (Palmeri et al. (2012)), the K-shell fluorescence yields for the K-vacancy fine-structure atomic levels of all the vanadium isonuclear ions have been calculated.

In this study, the K-shell EII cross sections connecting the ground and the metastable levels of the parent vanadium ions to the daughter ions K-vacancy levels considered in Palmeri et al. (2012) have been determined. The relativistic distorted-wave (DW) approximation implemented in the FAC atomic code has been used for the incident electron kinetic energies up to 20 times the K-shell threshold energies. Moreover, the resulting DW cross sections have been extrapolated at higher energies using the asymptotic behavior of the modified relativistic binary encounter Bethe model (MRBEB) of Guerra et al. (2012) with the density-effect correction proposed by Davies et al. (2013).

* Corresponding author.
E-mail addresses: patrick.palmeri@umons.ac.be (P. Palmeri), pascal.quinet@umons.ac.be (P. Quinet), batani@celia.u-bordeaux1.fr (D. Batani).

http://dx.doi.org/10.1016/j.adt.2015.04.002
0092-640X/

Contents

1. Introduction

The K-shell electron impact ionization (EII) cross section, along with the K-shell fluorescence yield, is one of the key atomic parameters for fast-electron diagnostic in laser–solid experiments through the K-shell emission cross section [1]. The study of fast electrons generated in these experiments is of interest, for instance, in shock ignition [2,3] and fast ignition [4,5] in inertial confinement fusion (ICF) and in energetic secondary particle production [6]. The Kα emission generated by the EII process is analyzed by either imagers which provide spatial and temporal information of relativistic electrons [7,8] or spectrometers, which provide bulk electron temperatures [9,10].

In particular, vanadium is an element, which has found a very large application in experiments concerning the physics of laser-produced plasmas and ICF. First, it has been used as an X-ray source for backlighting experiments. In the National Ignition Campaign [11] non-uniformity of irradiation and growth of hydro instabilities were studying imploding shells. These were radiographed with a vanadium backlighter, providing an X-ray source at 5.2 keV from He-α emission, and the growth of the perturbations was viewed with gated X-ray framing camera. Again V backlighters (5 μm thick foils) were used at NIF for laboratory astrophysics experiments [12] related to supersonic jet formation. Vanadium backlighters were also used in fast ignition experiments [13] and in high-energy density physics [14]. In this last case, the experiment performed at LULI 2000 aimed at determining the density of shocked plastic, and a two-dimensional monochromatic X-ray radiography was used, based on a spherical quartz crystal set to select the He-α line of vanadium and perform the image of the main target. The use of a monochromatic imager allows strongly reducing the noise associated to the intense plasma emission, partially superimposing to the He-α radiation used for radiography. This technique has been largely used, for instance Fujioka et al. [15] used it as a diagnostics for investigating implosion dynamics at the final stage of the fuel compression.

He-α emission from vanadium targets has also been used as a tracer layers. For instance in an early work to study the transport of energy in the overcritical plasma region [16] solid targets were uniformly illuminated at irradiances of 10^{14} to 10^{15} W/cm^2 and K-shell radiation was observed from vanadium coated with various layers of plastic. In a more recent experiment on the same topic, Schurtz et al. [17] have used emission from vanadium and titanium layers buried inside a target. The choice was due to the fact that the Ti and V He-α lines were easily identifiable and quite close to each other (5200 eV and 4800 eV) thereby the emission would correspond to similar temperature conditions reached at different depth inside the targets.

Concerning more specifically Kα emission from vanadium, a pioneering work [18] used it to measure local and remote energy deposition by fast electrons in planar targets irradiated by lasers with various pulse duration and wavelengths. Kα yield measurements allowed to study the lateral spreads of absorbed energy.

More recent experiments, performed after short-pulse high-intensity lasers have become available, used Kα emission yield of vanadium targets to estimate laser energy conversion to fast electrons from an electron transport model assuming a Maxwellian electron energy distribution [19–21]. The line ratio of Kα emission from a vanadium back layer with respect to the Kα emission from a titanium front layer has been used as a diagnostic of the fast electron temperature [22,23]. In these studies, the titanium front layer is used to absorb the laser photons and to cancel the contribution of the Kα emission of the vanadium back layer due to the K-shell photoionization process [22]. Akli et al. [24] studied the heating of solid targets irradiated by high-intensity lasers by X-ray spectroscopy of K-shell emission from thin Ni, Mo, and V layers. In this experiment, the front target layers were heated to $\sim$5 keV but the vanadium spectra showed cold Kα and Kβ but no thermal lines, suggesting that the rear-side temperature of the target was $<$400 eV.

During a campaign dedicated to the modeling of the K lines of astrophysical interest, the K-shell fluorescence yields for the K-vacancy fine-structure atomic levels of all the vanadium isonuclear ions have been calculated along with other fundamental decay parameters [25]. Moreover, the fine-structure effects on the iron K line shape with diagnostics implications have been studied in detail for astrophysical photoionized plasmas where the dominant process that populates K-vacancy levels is photoionization [26].

The purpose of this work is to provide the missing fine-structure K-shell EII cross sections required for modeling the V K lines produced in laser–solid experiments and that complement the decay data of Palmeri et al. [25] in order to take advantage of potential diagnostics of a fine-structure description.

2. Calculations

Following the method used in a previous study dedicated to the copper ions [27], the Flexible Atomic Code (FAC) [28] has been used to compute the EII cross sections by the relativistic distorted-wave (DW) method. In this method, the total EII cross section $\sigma_{ij}^{EII}(\varepsilon)$ (in atomic unit) from the initial fine-structure state ψ_i to the final ionized fine-structure state ψ_j at the incident electron kinetic energy ε is expressed in terms of the EII collision strength

$$\sigma_{ij}^{EII}(\varepsilon) = \frac{1}{k^2(2J_i+1)} \int_0^{\frac{\varepsilon - I_{ij}}{2}} \Omega_{ij}^{EII}(\varepsilon, \varepsilon')\, d\varepsilon' \tag{1}$$

$$\Omega_{ij}^{EII} = 2 \sum_{\kappa_i \kappa_j \kappa} \sum_{JJ_T} (2J_T+1) \times \left| \left\langle \psi_i\, \kappa_i, J_T M_T \left| \sum_{n<m} \frac{1}{r_{nm}} \right| (\psi_j\, \kappa) J\, \kappa_j, J_T M_T \right\rangle \right|^2 \tag{2}$$

where k is the incident electron kinetic momentum, J_i the total angular momentum of the target state ψ_i, ε' the kinetic energy

of the scattered electron, I_{ij} the threshold energy of the fine-structure transition $\psi_i \rightarrow \psi_j$, κ_i, κ_j, and κ the relativistic angular quantum numbers of respectively the incident, the scattered and the ejected electrons, J the total angular momentum resulting from the coupling of the final ionized state ψ_j and the ejected electron momentum κ, J_T the total angular momentum resulting from the coupling of J and the scattered electron momentum κ_j which must be equal to the coupling of the initial state ψ_i with the incident electron momentum κ_i, M_T the corresponding projection of J_T, i.e. the total magnetic quantum number. In addition, energy conservation imposes $\varepsilon = I_{ij} + \varepsilon' + \varepsilon''$ where ε'' is the kinetic energy of the ejected electron.

The N electron atomic state functions (ASF) $|\psi\rangle$ are superpositions of configuration state functions (CSF) $|\phi_v\rangle$ of the same conserved symmetries, i.e. parity, total angular momentum J_T and its projection M_T

$$|\psi\rangle = \sum_v a_v \, |\phi_v\rangle \tag{3}$$

where a_v are mixing coefficients determined by solving the secular equation of the N electron Dirac–Coulomb–Breit Hamiltonian.

The CSFs are antisymmetric sums of products of N one-electron Dirac spinors

$$\varphi_{n\kappa m} = \frac{1}{r}\begin{pmatrix} P_{n\kappa}(r)\ \chi_{\kappa m}(\theta,\phi,\sigma) \\ iQ_{n\kappa}(r)\ \chi_{-\kappa m}(\theta,\phi,\sigma) \end{pmatrix} \tag{4}$$

where the radial functions $P_{n\kappa}$ and $Q_{n\kappa}$ are respectively the large and small components and $\chi_{\kappa m}$ is the usual spin-angular function. n is the principal quantum number and κ is the relativistic angular quantum number which is related to the orbital l and the total angular momentum j of the electron through $\kappa = (l-j)(2j+1)$ where m is its magnetic quantum number. The radial functions are solutions of the Dirac–Fock–Slater (DFS) equations for the bound electrons where the local central potential is constructed using a fictitious mean configuration with fractional occupation numbers determined from the set of CSFs used to build the ASFs. The free electron radial functions are distorted-waves determined by solving the DFS equations using the same local central potential as for the bound orbitals.

In the present study, the target ASFs were built considering the same lists of configurations as in Ref. [25]. As the transition operator used in Eq. (2) is the Coulomb interaction operator, the high-energy rise of the EII cross section due to the Breit interaction (see e.g. Ref. [29]) will therefore not be taken into account by our FAC calculations. This relativistic rise starts at incident electron kinetic energy $\varepsilon \sim 100$ keV [30]. In order to consider this effect but also the density effect, the modified relativistic binary encounter Bethe (MRBEB) trend of Guerra et al. [30] (see Eqs. (5), (6) of this reference) is used with the density-effect correction proposed by Davies et al. [1] (see Eq. (7) of this reference). This resulting high-energy extrapolation replaces the empirical one used in our previous study on copper ions that was only valid for copper [27]. In neutral copper, it was shown that the MRBEB K-shell cross section corrected for the density effect better agrees with our RDW+Extrapol. model at high energy [27]. Concerning the density-effect correction ($\frac{\delta}{2}$), the values of the mean excitation energy ($I_{ex} = 245$ eV) and of the plasmon energy ($h\nu_p = 47.86$ eV) for vanadium are taken from the evaluations of Sternheimer et al. [31].

The resulting cross sections are expressed in barn using the following parametrized formula for each fine-structure transition $\psi_i \rightarrow \psi_j$:

$$\sigma_{ij}^{EII}(u) = \frac{3.80998406E+08}{(2J_i+1)\,u\,I_{ij}} \times \left\{ A_{ij}\,ln(u) + B_{ij}\left(1-\frac{1}{u}\right)^2 + \left(\frac{C_{ij}}{u}+\frac{D_{ij}}{u^2}\right)\left(1-\frac{1}{u}\right)\right\}$$

for $u \le u_0 = 20$

$$= K_{ij}\frac{5.10E+5}{I_{ij}} \times \left\{ \frac{1}{2}\left[ln\left(\frac{\gamma+1}{2}u\right) - \beta^2 - \frac{\delta}{2}\right] \times \left(1-\frac{1}{u^2}\right) + 1 - \frac{1}{u} + \left(\frac{2}{\gamma+1}\right)^2 \times \left[\frac{u-1}{2J^2} - (2\gamma-1)\frac{ln(u)}{1+u}\right]\right\} \times \left\{\beta^2 + (0.126 - 0.213Z + 0.195Z^2)\frac{2Ry}{I_{ij}}\beta_I^2\right\}^{-1}$$

for $u > u_0 = 20$ (5)

with

$$J = \frac{0.511E+06}{I_{ij}} \tag{6}$$

$$\gamma = 1 + \frac{u}{J} \tag{7}$$

$$\beta^2 = 1 - \frac{1}{\gamma^2} \tag{8}$$

$$\frac{\delta}{2} = ln\left[1 + (\gamma+1)\frac{h\nu_p}{I_{ex}}exp(-0.5)\right] \tag{9}$$

$$\beta_I^2 = 1 - \frac{1}{(1+1/J)^2} \tag{10}$$

where $u = \varepsilon/I_{ij}$ is the overpotential, A_{ij}, B_{ij}, C_{ij}, and D_{ij} are dimensionless coefficients fitted to the corresponding fine-structure DW cross sections calculated for $u \le 20$. The formula used for $u \le 20$ is the one given by Fontes et al. [32]. $Ry = 13.6056981$ eV is the Rydberg energy and Z(=23 for vanadium) is the atomic number. The extrapolation coefficient K_{ij} is the ratio between $\sigma_{ij}^{EII}(u=20)$ and the density-effect corrected MRBEB K-shell EII cross section evaluated at $u = 20$ used here for $u > 20$. In vanadium ions where 5.4 keV $\le I_{ij} \le$ 6.7 keV (see Table 2), an overpotential limit of $u_0 = 20$ corresponds to a kinetic energy limit of $\varepsilon_0 \sim 100$ keV where the Breit interaction effect becomes important. In Table 1, the 3953 vanadium ion fine-structure energy levels calculated by Palmeri et al. [25] to evaluate their decay properties are completed with the 119 fine-structure energy levels belonging to the ground complex $(3d+4s)^5$ of neutral vanadium that have been computed in this study using the same method as in Ref. [25]. Table 2 contains the K-shell EII cross section parameters used in Eq. (5) for the 15,834 fine-structure K-shell transitions between the levels reported in Table 1.

In Fig. 1, our calculated K-shell EII cross sections in V^0 are compared to the experimental data compiled by Liu et al. [35], the measurements of An et al. [36], the empirical XCVTS formula of Haque et al. [34], the combination of distorted-wave-Born and plane-wave-Born approximations (DWBA + PWBA) of Bote et al. [33], the MRBEB model of Guerra et al. [30] and this latter model corrected for the density effect as suggested by Davies et al. [1] (MRBEB + Density Effects). Our RDW + Extrapol. cross section curves are summations over all the fine-structure transitions from the V^0 ground level. The available experimental data [35,36] agree well with our model (RDW + Extrapol.) within their respective error bars. In addition, our RDW + Extrapol. cross section peaks at ~20 keV in agreement with all the available data except the XCVTS peak which is shifted by ~5 keV to the lower energies. Moreover, from threshold to the dip at ~10 MeV, our model follows the trend of the others (MRBEB, MRBEB + Density Effects, DWBA + PWBA and XCVTS) by better than ~20%. Beyond the dip, the density-effect correction proposed by Davies et al. [1] attenuates the relativistic rise of both the RDW + Extrapol. and

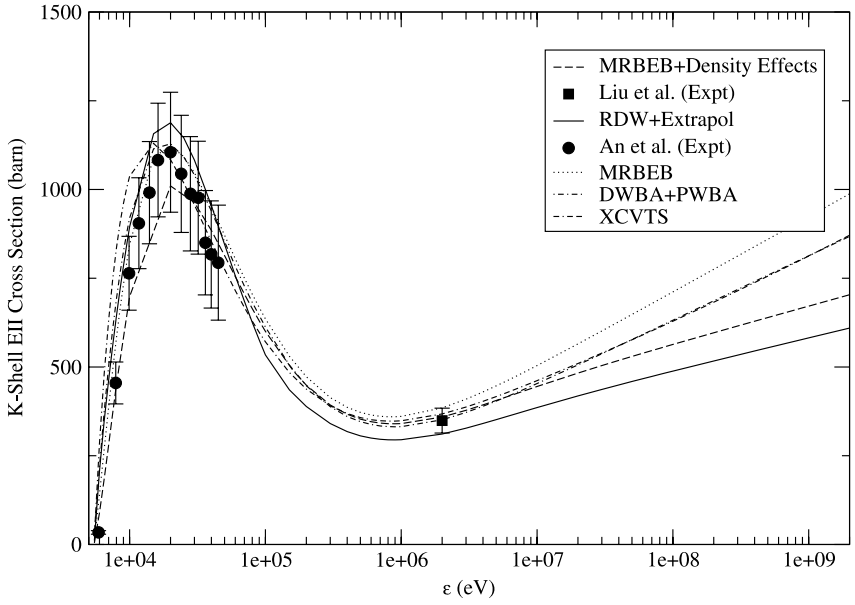

Fig. 1. Comparison of the DW + extrapol K-shell EII cross sections with experiment and other models in V^0. Solid line: DW + extrapol (this study); dot line: MRBEB model of Guerra et al. [30]; dash line: MRBEB model of Guerra et al. [30] with the density-effect correction proposed by Davies et al. [1]; dot–dash line: combination of distorted-wave-Born and plane-wave-Born approximations of Bote et al. [33]; dot–double-dash line: empirical XCVTS formula of Haque et al. [34]; full squares: compilation of experimental data by Liu et al. [35]; full circles: measurements by An et al. [36].

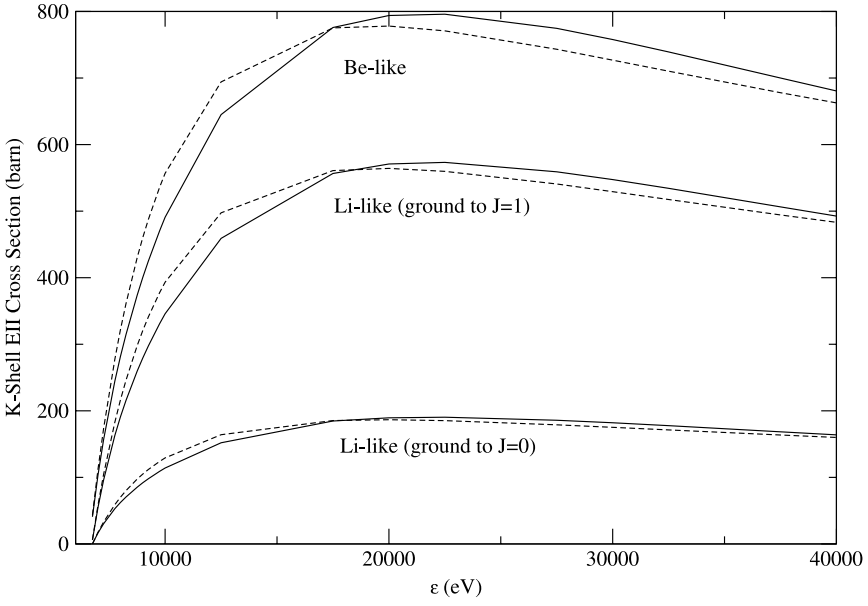

Fig. 2. Comparison of the K-shell EII cross sections in Li-like ($N = 3$) and Be-like ($N = 4$) V. Solid lines: DW calculations (this work) where only the Coulomb interaction is considered for the scattering matrix (see Eq. (2)). Dash lines: DW calculations of Fontes et al. [29] where the Breit interaction is taken into account. The Be-like curves are sums over all the fine-structure contributions from the ground level.

the MRBEB + Density effects cross sections compared to the other models (MRBEB, DWBA + PWBA and XCVTS). Unfortunately, there is no measurement here to constraint this high-energy trend.

In Fig. 2, our DW K-shell EII cross sections are compared in Li-like ($N = 3$) and Be-like ($N = 4$) vanadium with the DW fitted model of Fontes et al. [29] that takes into account the Breit interaction. The incident electron kinetic energy has been limited to 60 keV, i.e. $u \sim 6$, as suggested by Fontes et al. [29] as their fitted formulae are not expected to be reliable beyond that energy limit due to convergence problems in their DW calculations. The Be-like curves are sums over all the fine-structure contributions from the ground level. The agreements between our 'Coulomb only' model and the Coulomb–Breit model of Fontes et al. [29] are better than ∼20%. One can also notice the factor ∼3 difference between the fine-structure EII transitions $e^- + 1s^2 2s\ ^2S_{1/2} \rightarrow 1s2s\ ^1S_0 + 2e^-$ and $e^- + 1s^2 2s\ ^2S_{1/2} \rightarrow 1s2s\ ^3S_1 + 2e^-$.

3. Summary and conclusion

The K-shell EII cross sections have been calculated for 15,834 fine-structure transitions along the vanadium isonuclear sequence from V^0 up to V^{21+}. The DW method as implemented in the FAC atomic code [28] has been used for overpotentials of the incident electron up to $u = 20$. For $u > 20$, the cross sections have been extrapolated using the trend of the MRBEB K-shell EII cross section of Guerra et al. [30] with the density-effect correction proposed by Davies et al. [1]. The latters take into account both the Breit

interaction causing the high-energy relativistic rise as well as the density effect. These new ionization data in combination with the decay rates calculated by Palmeri et al. [25] should help to model the emissivities of the V K lines produced by fast-electron impacts in laser–solid experiments [37].

Acknowledgments

Financial support from the belgian FRS-FNRS is acknowledged. P.P. and P.Q. are respectively Research Associate and Research Director of this organization. The authors also acknowledge the support of the COST Action MP1208 "Developing the Physics and the Scientific Community for Inertial Fusion".

Appendix A. Supplementary data

Supplementary material related to this article can be found online at http://dx.doi.org/10.1016/j.adt.2015.04.002.

References

[1] J.R. Davies, R. Betti, P.M. Nilson, A.A. Solodov, Phys. Plasmas 20 (2013) 083118.
[2] S. Gus'kov, X. Ribeyre, M. Touati, J.L. Feugeas, Ph. Nicolaï, V. Tikhonchuk, Phys. Rev. Lett. 109 (2012) 255004.
[3] D. Batani, S. Baton, A. Casner, S. Depierreux, M. Hohenberger, O. Klimo, M. Koenig, C. Labaune, X. Ribeyre, C. Rousseaux, G. Schurtz, W. Theobald, V.T. Tikhonchuk, Nucl. Fusion 54 (2014) 054009.
[4] M. Tabak, J. Hammer, M.E. Glinsky, W.L. Kruer, S.C. Wilks, J. Woodworth, E.M. Campbell, M.D. Perry, R.J. Mason, Phys. Plasmas 1 (1994) 1626.
[5] P. Norreys, D. Batani, S. Baton, F. Beg, R. Kodama, Ph. Nilson, P. Patel, F. Perez, J.J. Santos, R. Scott, V.T. Tikhonchuk, M. Wei, J. Zhang, Nucl. Fusion 54 (2014) 054004.
[6] J.T. Mendonça, J.R. Davies, M. Eloy, Meas. Sci. Technol. 12 (2001) 1801.
[7] P.M. Nilson, J.R. Davies, W. Theobald, P.A. Jaanimagi, C. Mileham, R.K. Jungquist, C. Stoeckl, I.A. Begishev, A.A. Solodov, J.F. Myatt, J.D. Zuegel, T.C. Sangster, R. Betti, D.D. Meyerhofer, Phys. Rev. Lett. 108 (2012) 085002.
[8] A. Morace, D. Batani, Nucl. Instrum. Methods Phys. Res. A 623 (2010) 797.
[9] W. Theobald, K. Akli, R. Clarke, J.A. Delettrez, R.R. Freeman, S. Glenzer, J. Green, G. Gregori, R. Heathcote, N. Izumi, J.A. King, J.A. Koch, J. Kuba, K. Lancaster, A.J. MacKinnon, M. Key, C. Mileham, J. Myatt, D. Neely, P.A. Norreys, H.-S. Park, J. Pasley, P. Patel, S.P. Regan, H. Sawada, R. Shepherd, R. Snavely, R.B. Stephens, C. Stoeckl, M. Storm, B. Zhang, T.C. Sangster, Phys. Plasmas 13 (2006) 043102.
[10] E. Martinolli, M. Koenig, S.D. Baton, J.J. Santos, F. Amiranoff, D. Batani, E. Perelli-Cippo, F. Scianitti, L. Gremillet, C. Rousseaux, T.A. Hall, M.H. Key, R. Snavely, A. MacKinnon, R.R. Freeman, J.A. King, D. Neely, R.J. Clark, Phys. Rev. E 73 (2006) 046402.
[11] J. Lindl, O. Landen, J. Edwards, E. Moses, NIC Team, Phys. Plasmas 21 (2014) 020501.
[12] B.E. Blue, S.V. Weber, S.G. Glendinning, N.E. Lanier, D.T. Woods, M.J. Bono, S.N. Dixit, C.A. Haynam, J.P. Holder, D.H. Kalantar, B.J. MacGowan, A.J. Nikitin, V.V. Rekow, B.M. Van Wonterghem, E.I. Moses, P.E. Stry, B.H. Wilde, W.W. Hsing, H.F. Robey, Phys. Rev. Lett. 94 (2005) 095005.
[13] S.P. Hatchett, D. Clark, M. Tabak, R.E. Turner, C. Stoeckl, R.B. Stephens, H. Shiraga, K. Tanaka, Fusion Sci. Technol. 49 (2006) 327.
[14] A. Benuzzi-Mounaix, B. Loupias, M. Koenig, A. Ravasio, N. Ozaki, M. Rabec le Gloahec, T. Vinci, Y. Aglitskiy, A. Faenov, T. Pikuz, T. Boehly, Phys. Rev. E 77 (2008) 045402R.
[15] S. Fujioka, T. Fujiwara, M. Tanabe, H.H. Nishimura, H. Nagamoto, S. Ohira, Y. Inubushi, H. Shiraga, H. Azechi, Rev. Sci. Instrum. 81 (2010) 10E529.
[16] A. Hauer, W.C. Mead, O. Willi, J.D. Kilkenny, D.K. Bradley, S.D. Tabatabaei, C. Hooker, Phys. Rev. Lett. 53 (1984) 2563.
[17] G. Schurtz, S. Gary, S. Hulin, C. Chenais-Popovics, J.-C. Gauthier, F. Thais, J. Breil, F. Durut, J.-L. Feugeas, P.-H. Maire, P. Nicolaï, O. Peyrusse, C. Reverdin, G. Soullié, V. Tikhonchuk, B. Villette, C. Fourment, Phys. Rev. Lett. 98 (2007) 095002.
[18] F. Amiranoff, K. Eidmann, R. Sigel, R. Fedosejevs, A. Maaswink, Y.-L. Teng, J.D. Kilkenny, J.D. Hares, D.K. Bradley, J. MacGowan, T.J. Goldsack, J. Phys. D: Appl. Phys. 15 (1982) 2463.
[19] J.C. Kieffer, H. Pépin, F. Amiranoff, Appl. Phys. Lett. 44 (1984) 494.
[20] D. Jung, L.A. Gizzi, L. Labate, D. Neely, M.N. Notley, P.P. Rajeev, M. Roth, G. Gregori, Phys. Rev. E 77 (2008) 056403.
[21] Z. Jiang, J.C. Kieffer, J.P. Matte, M. Chaker, O. Peyrusse, D. Gilles, G. Korn, A. Maksimchuk, S. Coe, G. Mourou, Phys. Plasmas 2 (1995) 1702.
[22] B. Yaakobi, C. Stoekl, T. Boehly, D.D. Meyerhofer, W. Seka, Phys. Plasmas 7 (2000) 3714.
[23] C. Stoekl, R.E. Bahr, B. Yaakobi, W. Seka, S.P. Regan, R.S. Craxton, J.A. Delettrez, R.W. Short, J. Myatt, A.V. Maximov, H. Baldis, Phys. Rev. Lett. 90 (2003) 235002.
[24] K.U. Akli, S.B. Hansen, A.J. Kemp, R.R. Freeman, F.N. Beg, D.C. Clark, S.D. Chen, D. Hey, S.P. Hatchett, K. Highbarger, R. Giraldez, J.S. Green, G. Gregori, K.L. Lancaster, T. Ma, J. MacKinnon, P. Norreys, N. Patel, J. Pasley, C. Shearer, R.B. Stephens, C. Stoekl, M. Storm, W. Theobald, L.D. Van Woerkom, R. Weber, M.H. Keyl, Phys. Rev. Lett. 100 (2008) 165002.
[25] P. Palmeri, P. Quinet, C. Mendoza, M.A. Bautista, J. García, M.C. Witthoeft, T.R. Kallman, Astronom. Astrophys. 543 (2012) A44.
[26] T.R. Kallman, P. Palmeri, M.A. Bautista, C. Mendoza, J.H. Korlik, Astrophys. J. Suppl. Ser. 155 (2004) 675.
[27] P. Palmeri, P. Quinet, D. Batani, At. Data Nucl. Data Tables 102 (2015) 1.
[28] M.F. Gu, Astrophys. J. 582 (2003) 1241.
[29] C.J. Fontes, D.H. Sampson, H.L. Zhang, Phys. Rev. A 59 (1999) 1329.
[30] M. Guerra, F. Parente, P. Indelicato, J.P. Santos, Int. J. Mass Spectrom. 313 (2012) 1.
[31] R.M. Sternheimer, S.M. Seltzer, M.J. Berger, Phys. Rev. B 26 (1982) 6067.
[32] C.J. Fontes, D.H. Sampson, H.L. Zhang, Phys. Rev. A 48 (1993) 1975.
[33] D. Bote, F. Salvat, A. Jablonski, C.J. Powell, At. Data Nucl. Data Tables 95 (2009) 871.
[34] A.K.F. Haque, M.R. Talukder, M. Shahjahan, M.A. Uddin, A.K. Basak, B.C. Saha, J. Phys. B 43 (2010) 115201.
[35] M. Liu, Z. An, C. Tang, Z. Luo, X. Peng, X. Long, At. Data Nucl. Data Tables 76 (2000) 213.
[36] Z. An, C.H. Tang, C.G. Zhou, Z.M. Luo, J. Phys. B 33 (2000) 3677.
[37] H.-K. Chung, M.H. Chen, R.W. Lee, High Energy Density Phys. 3 (2007) 57.

Explanation of Tables

Table 1. Fine-Structure Energy Levels in the Vanadium Isonuclear Sequence, from V^0 to V^{21+}.
The fine-structure energy levels of V^0–V^{21+} considered in the K-shell EII cross sections presented in Table 2. This table is based on Table 9 of Ref. [25]. Except for neutral vanadium where new HFR values are given, the configuration assignments and energies shown are those calculated by Palmeri et al. [25] using the HFR method. This is a sample of the table where only the data for $N = 2$–4 are given. The complete table is provided as a supplementary MS-Excel file.

N	The number of electrons of the vanadium ion
i	The fine-structure level index
$2S + 1$	The level multiplicity
L	The level total orbital angular momentum quantum number
$2J$	Two times the level total angular momentum quantum number
Configuration	The level configuration assignment
E (eV)	The level energy in eV

Table 2. Parameters for the Fine-Structure K-shell EII Cross Sections in the Vanadium Isonuclear Sequence, from V^0 to V^{21+}.
This table presents the parameters used in Eq. (5) for each fine-structure K-shell transition $i \rightarrow j$ between the parent (N) and daughter (N') vanadium ions. This is a sample of the table where only the data for $N = 3$–4 are given. The complete table is provided as a supplementary MS-Excel file.

N	The number of electrons of the parent vanadium ion (see Table 1)
i	The parent ion level index (see Table 1)
N'	The number of electrons of the daughter vanadium ion (see Table 1)
j	The daughter ion level index (see Table 1)
$2J_i + 1$	The statistical weight of the parent ion level i
I_{ij} (eV)	The threshold energy for the fine-structure transition $i \rightarrow j$ (in eV)
A_{ij}	The A_{ij} coefficient of Eq. (5)
B_{ij}	The B_{ij} coefficient of Eq. (5)
C_{ij}	The C_{ij} coefficient of Eq. (5)
D_{ij}	The D_{ij} coefficient of Eq. (5)
K_{ij}	The extrapolation coefficient K_{ij} of Eq. (5)

Table 1
Fine-Structure Energy Levels in the Vanadium Isonuclear Sequence, from V^0 to V^{21+} (this is a sample where only the data for $N = 2$–4 are given).

N	i	$2S+1$	L	$2J$	Configuration	E (eV)
2	1	1	0	0	$1s^2$ (^{1}S) ^{1}S	0.0000E+00
2	2	3	0	2	1s2s (^{2}S) ^{3}S	5.1546E+03
2	3	3	1	0	1s2p (^{2}S) ^{3}P	5.1783E+03
2	4	3	1	2	1s2p (^{2}S) ^{3}P	5.1809E+03
2	5	1	0	0	1s2s (^{2}S) ^{1}S	5.1813E+03
2	6	3	1	4	1s2p (^{2}S) ^{3}P	5.1894E+03
2	7	1	1	2	1s2p (^{2}S) ^{1}P	5.2064E+03
3	1	2	0	1	$1s^2$2s (^{1}S) ^{2}S	0.0000E+00
3	2	2	1	1	$1s^2$2p (^{1}S) ^{2}P	4.2177E+01
3	3	2	1	3	$1s^2$2p (^{1}S) ^{2}P	5.1561E+01
3	4	2	0	1	1s$2s^2$ (^{2}S) ^{2}S	5.1227E+03
3	5	4	1	1	1s2s2p (^{3}S) ^{4}P	5.1324E+03
3	6	4	1	3	1s2s2p (^{3}S) ^{4}P	5.1356E+03
3	7	4	1	5	1s2s2p (^{3}S) ^{4}P	5.1422E+03
3	8	2	1	1	1s2s2p (^{1}S) ^{2}P	5.1676E+03
3	9	2	1	3	1s2s2p (^{3}S) ^{2}P	5.1732E+03
3	10	4	1	1	1s$2p^2$ (^{3}P) ^{4}P	5.1810E+03
3	11	4	1	3	1s$2p^2$ (^{3}P) ^{4}P	5.1854E+03
3	12	2	1	1	1s2s2p (^{3}S) ^{2}P	5.1857E+03
3	13	2	1	3	1s2s2p (^{1}S) ^{2}P	5.1877E+03
3	14	4	1	5	1s$2p^2$ (^{3}P) ^{4}P	5.1903E+03
3	15	2	2	3	1s$2p^2$ (^{1}D) ^{2}D	5.2078E+03
3	16	2	1	1	1s$2p^2$ (^{3}P) ^{2}P	5.2108E+03
3	17	2	2	5	1s$2p^2$ (^{1}D) ^{2}D	5.2109E+03
3	18	2	1	3	1s$2p^2$ (^{3}P) ^{2}P	5.2208E+03
3	19	2	0	1	1s$2p^2$ (^{1}S) ^{2}S	5.2397E+03
4	1	1	0	0	$2s^2$ (^{1}S) ^{1}S	0.0000E+00
4	2	3	1	0	2s2p (^{2}S) ^{3}P	3.7465E+01
4	3	3	1	2	2s2p (^{2}S) ^{3}P	4.0010E+01
4	4	3	1	4	2s2p (^{2}S) ^{3}P	4.6526E+01
4	5	1	1	2	2s2p (^{2}S) ^{1}P	7.8875E+01
4	6	3	1	0	$2p^2$ (^{3}P) ^{3}P	1.0167E+02
4	7	3	1	2	$2p^2$ (^{3}P) ^{3}P	1.0619E+02
4	8	3	1	4	$2p^2$ (^{3}P) ^{3}P	1.1045E+02
4	9	1	2	4	$2p^2$ (^{1}D) ^{1}D	1.2255E+02
4	10	1	0	0	$2p^2$ (^{1}S) ^{1}S	1.4705E+02
4	11	3	1	0	[1s]$2s^2$2p (^{2}S) ^{3}P	5.1181E+03
4	12	3	1	2	[1s]$2s^2$2p (^{2}S) ^{3}P	5.1205E+03
4	13	3	1	4	[1s]$2s^2$2p (^{2}S) ^{3}P	5.1280E+03
4	14	5	1	2	[1s]2s$2p^2$ (^{3}P) ^{5}P	5.1314E+03
4	15	5	1	4	[1s]2s$2p^2$ (^{3}P) ^{5}P	5.1355E+03
4	16	5	1	6	[1s]2s$2p^2$ (^{3}P) ^{5}P	5.1403E+03
4	17	1	1	2	[1s]$2s^2$2p (^{2}S) ^{1}P	5.1442E+03
4	18	3	1	0	[1s]2s$2p^2$ (^{3}P) ^{3}P	5.1719E+03
4	19	3	2	2	[1s]2s$2p^2$ (^{3}P) ^{3}P	5.1736E+03
4	20	3	2	4	[1s]2s$2p^2$ (^{1}D) ^{3}D	5.1747E+03
4	21	3	2	6	[1s]2s$2p^2$ (^{1}D) ^{3}D	5.1771E+03
4	22	3	2	2	[1s]2s$2p^2$ (^{1}D) ^{3}D	5.1774E+03
4	23	3	1	4	[1s]2s$2p^2$ (^{3}P) ^{3}P	5.1821E+03
4	24	3	0	2	[1s]2s$2p^2$ (^{1}S) ^{3}S	5.1934E+03
4	25	3	1	0	[1s]2s$2p^2$ (^{3}P) ^{3}P	5.1961E+03
4	26	1	2	4	[1s]2s$2p^2$ (^{1}D) ^{1}D	5.2003E+03
4	27	3	1	2	[1s]2s$2p^2$ (^{3}P) ^{3}P	5.2027E+03
4	28	5	0	4	[1s]$2p^3$ (^{4}S) ^{5}S	5.2038E+03
4	29	3	1	4	[1s]2s$2p^2$ (^{3}P) ^{3}P	5.2076E+03
4	30	1	1	2	[1s]2s$2p^2$ (^{3}P) ^{1}P	5.2192E+03
4	31	1	0	0	[1s]2s$2p^2$ (^{1}S) ^{1}S	5.2231E+03
4	32	3	2	2	[1s]$2p^3$ (^{2}D) ^{3}D	5.2295E+03
4	33	3	2	4	[1s]$2p^3$ (^{2}D) ^{3}D	5.2300E+03
4	34	3	2	6	[1s]$2p^3$ (^{2}D) ^{3}D	5.2316E+03
4	35	3	0	2	[1s]$2p^3$ (^{4}S) ^{3}S	5.2392E+03
4	36	1	2	4	[1s]$2p^3$ (^{2}D) ^{1}D	5.2463E+03
4	37	3	1	0	[1s]$2p^3$ (^{2}P) ^{3}P	5.2489E+03
4	38	3	1	2	[1s]$2p^3$ (^{2}P) ^{3}P	5.2509E+03
4	39	3	1	4	[1s]$2p^3$ (^{2}P) ^{3}P	5.2555E+03
4	40	1	1	2	[1s]$2p^3$ (^{2}P) ^{1}P	5.2695E+03

Table 2
Parameters for the Fine-Structure K-shell EII Cross Sections in the Vanadium Isonuclear Sequence, from V^0 to V^{21+} (this is a sample where only the data for $N = 3$–4 are given).

N	i	N'	j	$2J_i + 1$	I_{ij} (eV)	A_{ij}	B_{ij}	C_{ij}	D_{ij}	K_{ij}
3	1	2	2	2.0000E+00	6.7221E+03	2.2979E−02	1.0424E−01	-8.9362E−02	1.1828E−01	5.6013E−01
3	1	2	5	2.0000E+00	6.7488E+03	7.6597E−03	3.4752E−02	-2.9725E−02	3.9350E−02	1.8728E−01
3	2	2	3	2.0000E+00	6.7047E+03	7.6594E−03	3.4742E−02	-2.9828E−02	3.9478E−02	1.8633E−01
3	2	2	4	2.0000E+00	6.7063E+03	1.9787E−02	8.9754E−02	-7.7049E−02	1.0198E−01	4.8146E−01
3	2	2	7	2.0000E+00	6.7308E+03	3.1909E−03	1.4476E−02	-1.2401E−02	1.6414E−02	7.7859E−02
3	3	2	4	4.0000E+00	6.6970E+03	3.1908E−03	1.4473E−02	-1.2434E−02	1.6455E−02	3.8779E−02
3	3	2	6	4.0000E+00	6.7054E+03	3.8297E−02	1.7371E−01	-1.4913E−01	1.9738E−01	4.6587E−01
3	3	2	7	4.0000E+00	6.7216E+03	1.9788E−02	8.9763E−02	-7.6956E−02	1.0186E−01	2.4116E−01
4	1	3	4	1.0000E+00	6.6081E+03	1.6135E−02	6.9797E−02	-6.1243E−02	7.9855E−02	7.5593E−01
4	1	3	10	1.0000E+00	6.6680E+03	1.8645E−05	8.0684E−05	-7.0462E−05	9.1880E−05	8.7960E−04
4	1	3	16	1.0000E+00	6.6956E+03	5.1008E−06	2.2076E−05	-1.9239E−05	2.5086E−05	2.4139E−04
4	1	3	19	1.0000E+00	6.7249E+03	6.4970E−05	2.8124E−04	-2.4455E−04	3.1886E−04	3.0850E−03
4	2	3	5	1.0000E+00	6.5811E+03	1.1663E−02	5.0442E−02	-4.4357E−02	5.7834E−02	5.4469E−01
4	2	3	8	1.0000E+00	6.6144E+03	4.5522E−03	1.9692E−02	-1.7270E−02	2.2518E−02	2.1342E−01
4	2	3	12	1.0000E+00	6.6335E+03	8.6270E−06	3.7324E−05	-3.2683E−05	4.2617E−05	4.0537E−04
4	3	3	5	3.0000E+00	6.5787E+03	4.5598E−03	1.9721E−02	-1.7345E−02	2.2615E−02	7.0965E−02
4	3	3	6	3.0000E+00	6.5811E+03	2.9121E−02	1.2595E−01	-1.1075E−01	1.4440E−01	4.5334E−01
4	3	3	8	3.0000E+00	6.6120E+03	1.1623E−02	5.0279E−02	-4.4103E−02	5.7507E−02	1.8159E−01
4	3	3	9	3.0000E+00	6.6174E+03	2.9574E−03	1.2794E−02	-1.1217E−02	1.4626E−02	4.6235E−02
4	3	3	12	3.0000E+00	6.6311E+03	4.1201E−05	1.7825E−04	-1.5612E−04	2.0357E−04	6.4514E−04
4	3	3	13	3.0000E+00	6.6328E+03	3.6955E−04	1.5988E−03	-1.4001E−03	1.8256E−03	5.7877E−03
4	4	3	6	5.0000E+00	6.5746E+03	3.3267E−03	1.4387E−02	-1.2658E−02	1.6504E−02	3.1049E−02
4	4	3	7	5.0000E+00	6.5811E+03	4.8671E−02	2.1050E−01	-1.8511E−01	2.4135E−01	4.5461E−01
4	4	3	9	5.0000E+00	6.6109E+03	2.5987E−02	1.1241E−01	-9.8613E−02	1.2858E−01	2.4357E−01
4	4	3	13	5.0000E+00	6.6264E+03	3.1349E−03	1.3562E−02	-1.1883E−02	1.5494E−02	2.9436E−02
4	5	3	5	3.0000E+00	6.5393E+03	8.3524E−07	3.6113E−06	-3.1867E−06	4.1543E−06	1.2938E−05
4	5	3	6	3.0000E+00	6.5417E+03	9.0016E−08	3.8921E−07	-3.4338E−07	4.4765E−07	1.3948E−06
4	5	3	8	3.0000E+00	6.5726E+03	4.8990E−05	2.1187E−04	-1.8644E−04	2.4308E−04	7.6189E−04
4	5	3	9	3.0000E+00	6.5780E+03	3.5042E−03	1.5155E−02	-1.3330E−02	1.7380E−02	5.4531E−02
4	5	3	12	3.0000E+00	6.5917E+03	1.6174E−02	6.9957E−02	-6.1464E−02	8.0141E−02	2.5210E−01
4	5	3	13	3.0000E+00	6.5935E+03	2.8944E−02	1.2519E−01	-1.0998E−01	1.4339E−01	4.5123E−01
4	6	3	4	1.0000E+00	6.5055E+03	2.1528E−05	9.3059E−05	-8.2353E−05	1.0734E−04	9.9644E−04
4	6	3	10	1.0000E+00	6.5654E+03	1.2155E−02	5.2564E−02	-4.6283E−02	6.0342E−02	5.6661E−01
4	6	3	16	1.0000E+00	6.5930E+03	4.0331E−03	1.7444E−02	-1.5325E−02	1.9982E−02	1.8861E−01
4	6	3	19	1.0000E+00	6.6223E+03	1.3930E−05	6.0263E−05	-5.2817E−05	6.8870E−05	6.5370E−04
4	7	3	4	3.0000E+00	6.5010E+03	6.1557E−07	2.6608E−06	-2.3556E−06	3.0704E−06	9.4922E−06
4	7	3	10	3.0000E+00	6.5609E+03	4.0473E−03	1.7502E−02	-1.5416E−02	2.0099E−02	6.2856E−02
4	7	3	11	3.0000E+00	6.5653E+03	2.8859E−02	1.2480E−01	-1.0989E−01	1.4327E−01	4.4842E−01
4	7	3	15	3.0000E+00	6.5868E+03	1.1988E−03	5.1850E−03	-4.5574E−03	5.9422E−03	1.8675E−02
4	7	3	16	3.0000E+00	6.5885E+03	1.2093E−02	5.2305E−02	-4.5967E−02	5.9934E−02	1.8842E−01
4	7	3	18	3.0000E+00	6.5989E+03	2.3893E−03	1.0335E−02	-9.0748E−03	1.1832E−02	3.7273E−02
4	7	3	19	3.0000E+00	6.6178E+03	8.2749E−05	3.5797E−04	-3.1385E−04	4.0924E−04	1.2937E−03
4	8	3	11	5.0000E+00	6.5612E+03	3.4451E−03	1.4898E−02	-1.3122E−02	1.7108E−02	3.2104E−02
4	8	3	14	5.0000E+00	6.5653E+03	4.8144E−02	2.0820E−01	-1.8332E−01	2.3901E−01	4.4885E−01
4	8	3	15	5.0000E+00	6.5828E+03	1.5765E−02	6.8182E−02	-5.9949E−02	7.8163E−02	1.4728E−01
4	8	3	17	5.0000E+00	6.5853E+03	5.2673E−04	2.2781E−03	-2.0026E−03	2.6111E−03	4.9222E−03
4	8	3	18	5.0000E+00	6.5948E+03	1.3238E−02	5.7258E−02	-5.0295E−02	6.5578E−02	1.2385E−01
4	9	3	11	5.0000E+00	6.5488E+03	1.4293E−04	6.1801E−04	-5.4491E−04	7.1040E−04	1.3299E−03
4	9	3	14	5.0000E+00	6.5529E+03	5.2672E−04	2.2776E−03	-2.0075E−03	2.6172E−03	4.9035E−03
4	9	3	15	5.0000E+00	6.5703E+03	1.5484E−02	6.6962E−02	-5.8936E−02	7.6840E−02	1.4444E−01
4	9	3	17	5.0000E+00	6.5728E+03	4.8144E−02	2.0821E−01	-1.8322E−01	2.3888E−01	4.4925E−01
4	9	3	18	5.0000E+00	6.5824E+03	1.6821E−02	7.2749E−02	-6.3966E−02	8.3401E−02	1.5714E−01
4	10	3	4	1.0000E+00	6.4595E+03	6.6554E−05	2.8759E−04	-2.5553E−04	3.3298E−04	3.0635E−03
4	10	3	10	1.0000E+00	6.5194E+03	2.5410E−06	1.0985E−05	-9.7098E−06	1.2657E−05	1.1781E−04
4	10	3	16	1.0000E+00	6.5470E+03	9.2533E−05	4.0011E−04	-3.5283E−04	4.5998E−04	4.3042E−03
4	10	3	19	1.0000E+00	6.5764E+03	1.6062E−02	6.9465E−02	-6.1109E−02	7.9675E−02	7.4971E−01